Available online at www.sciencedirect.com
ScienceDirect
International Journal of Heat and Mass Transfer 51 (2008) 389–396
International Journal of HEAT and MASS TRANSFER
www.elsevier.com/locate/ijhmt

Technical Note

Effect of pulse heating parameters on the microscale bubble dynamics at a microheater surface

Jinliang Xu [a,*], Wei Zhang [a,b]

[a] Micro Energy System Laboratory, Key Laboratory of Renewable Energy and Gas Hydrate, Guangzhou Institute of Energy Conversion, Chinese Academy of Sciences, Guangzhou 510640, PR China
[b] Graduate University of Chinese Academy of Science, Beijing 100039, PR China

Received 8 December 2006; received in revised form 4 September 2007
Available online 23 October 2007

Abstract

We study the effects of pulse heating parameters on the micro bubble behavior of a platinum microheater (100 μm×20 μm) immersed in a methanol pool. The experiment covers the heat fluxes of 10–37 MW/m^2 and pulse frequencies of 25–500 Hz. The boiling incipience is initiated at the superheat limit of methanol, corresponding to the homogeneous nucleation. Three types of micro boiling patterns are identified. The first type is named as the bubble explosion and regrowth, consisting of a violent explosive boiling and shrinking, followed by a slower bubble regrowth and subsequent shrinking, occurring at lower heat fluxes. The second type, named as the bubble breakup and attraction, consists of the violent explosive boiling, bubble breakup and emission, bubble attraction and coalescence process, occurring at higher heat fluxes than those of the first type. The third type, named as the bubble size oscillation and large bubble formation, involves the initial explosive boiling, followed by a short periodic bubble growth and shrinking. Then the bubble continues to increase its size, until a constant bubble size is reached which is larger than the microheater length.

Keywords: Pulse heating parameter; Explosive boiling; Bubble breakup and emission; Bubble attraction and coalescence

1. Introduction

Since the commercial application of the ink-jet printer, microscale bubble dynamics has been received great attention. The bubble-powered actuators have the distinct advantages over other types of actuation sources in microscale due to operation in low voltages, easy implementation by using resistive heaters without mechanical microstructures [1]. Although the boiling process can be observed in our daily life and has many applications, control of the bubble generation and collapse can only be fulfilled in microscale. The recent developments include the bubble-powered nozzle-diffuser pumps [2], the bubble-powered micro-mixer [3], the periodic bubble generation and collapse for DNA actuators [4], etc.

One of the most important issues of the microscale bubble dynamics is to determine the boiling incipience temperature. According to the classical bubble nucleation theory, liquid temperature should reach 0.9 T_c to trigger the boiling incipience [5]. Several factors affect the bubble nucleation temperature at the microheater surface: the non-condensation gas dissolved in liquid, the heater surface roughness, and the heating rates.

Many studies deal with the micro bubble behavior under the pulse heating mode. These studies can be categorized into two groups: the homogeneous nucleation and the heterogeneous nucleation. Asai [6] demonstrated that the measured boiling incipience temperature is consistent with the homogeneous nucleation theory by the deviation of 5–15 K with the microheater immersed in methanol liquid. Glod et al. [7] used a short (1 mm in length) and ultrathin (10 μm in diameter) platinum wire with the pulse heating to study the explosive boiling using water as the working

* Corresponding author. Tel./fax: +86 20 87057656.
E-mail address: xujl@ms.giec.ac.cn (J. Xu).

0017-9310/$ - see front matter © 2007 Elsevier Ltd. All rights reserved.
doi:10.1016/j.ijheatmasstransfer.2007.09.007

Nomenclature

f	pulse heating frequency, Hz
L	microheater length, m or μm
Q	joule heat created by the microheater, W
q	heat flux on the microheater, W/m^2 or MW/m^2
R_{Au1}, R_{Au2}	the left and right gold pad resistance, Ω
R_{Pt}	the platinum film resistance, Ω
R_s	the selected resistance from the precision resistance box, Ω
T_c	critical temperature of fluid, K
T_{cycle}	cycle period of the pulse heating signal, s or ms
T_{Pt}	microheater temperature, °C or K
t	time, s or ms
V_1	dc voltage applied to the microheater and its two gold pads, V
V_2	dc voltage applied to the precise resistance, V
W	microheater width, m or μm
x, y	x and y coordinates for the bubble attraction phenomenon, m or μm
τ_1	pulse duration time of the heating pulse, ms or s
τ_2	waiting time of the heating pulse during which the voltage is zero, ms or s
Δx_i	uncertainty of the parameter x_i

fluid. They found that either the homogeneous or the heterogeneous nucleation could occur, depending on the heating rates. When the heating rate exceeds about 60×10^6 K/s, the measured boiling incipience temperature is 303 °C, consistent well with the homogeneous superheat limit of water. The heterogeneous micro boiling was performed by Li and Peterson [8], with the platinum heater size of 100 × 100 μm. They found that the explosive boiling can take place on a smooth heater no matter how slow the heating speed is, and the dissolved gas plays a significant role on the boiling incipience and bubble behavior.

The homogeneous nucleation temperature limit was observed by Chen et al. [9] using a 96 individual microheater array with the size of 270 × 270 μm for each. However, the boiling process can be maintained at a lower superheat after the explosive boiling, attributed to the necking embryo during the bubble departure from which the next generation bubbles grow. The microheater size effect on the bubble dynamics was performed by Deng et al. [10], in which the heater size of 10 μm is found to be a critical value.

In this paper, we fabricated a microheater by the size of 100 × 20 μm on a 7740 glass wafer. It is found that the homogeneous nucleation governs the boiling incipience. The micro boiling can be categorized into three types. The first type is the repeated explosive boiling followed by the bubble regrowth, occurring at lower heat fluxes. The higher heat flux results in a successive of the explosive boiling, bubble breakup and emission, bubble attraction and coalescence process. Sufficient high heat fluxes or high pulse frequencies yield the initial periodic bubble growth and shrinking, followed by a slow continuous bubble growth until a subsequent constant bubble size is reached.

2. The microheater test section and experimental facilities

The microheater is shown in Fig. 1a. The photoresist was spun on a 7740 Pyrex glass wafer. After patterning with the technique of photolithography, a titanium layer of 200 Å, a platinum layer of 1500 Å and a gold layer of 3000 Å were sputtered successively on the wafer. After another process of photolithography, the technique of chemical etching was used to remove the gold corresponding to the position of the platinum microheater. The platinum heater area is 100 μm in length and 20 μm in width.

The methanol was boiled for more than half hour to remove any non-condensable gas and then cooled down to the room temperature. During the experiment, an open glass beaker contains the methanol liquid. The microheater wafer is horizontally positioned in the methanol pool. The vertical distance between the glass wafer plane and the top liquid surface is about 10 mm. Even though the heat flux at the microheater surface is high, the total heating power is significant small, which has not any influence on the liquid pool temperature. The produced vapor is periodically condensed by the surrounding subcooled liquid.

Fig. 1b shows the experimental setup. An EE1641C function generator was used to generate the rectangular pulse voltage that was applied to the microheater, which has the output frequencies from 0.2 Hz to 20 MHz, and the output voltage amplitude from 0 to 20 V. A precision resistance box provides a selective, precision external resistance that was connected with the microheater. Because the resistance is known, the current that is flowing through the microheater circuit can be obtained by measuring the voltage across the resistance. In the present experiment, the DL750 high speed data acquisition system measures the liquid pool temperature, and the two dc voltages that were applied to the microheater and its connected resistance, with the recording rate of 10 M samples per second.

The Leica MZ16 stereo-microscope was bonded with a high speed camera. In the present experiment, we use the high speed recording rate of 20,000 fps. The microheater length of 100 μm corresponds to 100 pixels in the visualization area. Thus the spatial resolution of the optical system is 1 μm per pixel. The maximum uncertainty of the data acquisition system for the voltage measurement is 1 mV.

During the experiment, both the high speed data acquisition system and the high speed camera are in the waiting mode. The synchronization hub sends a signal, triggering

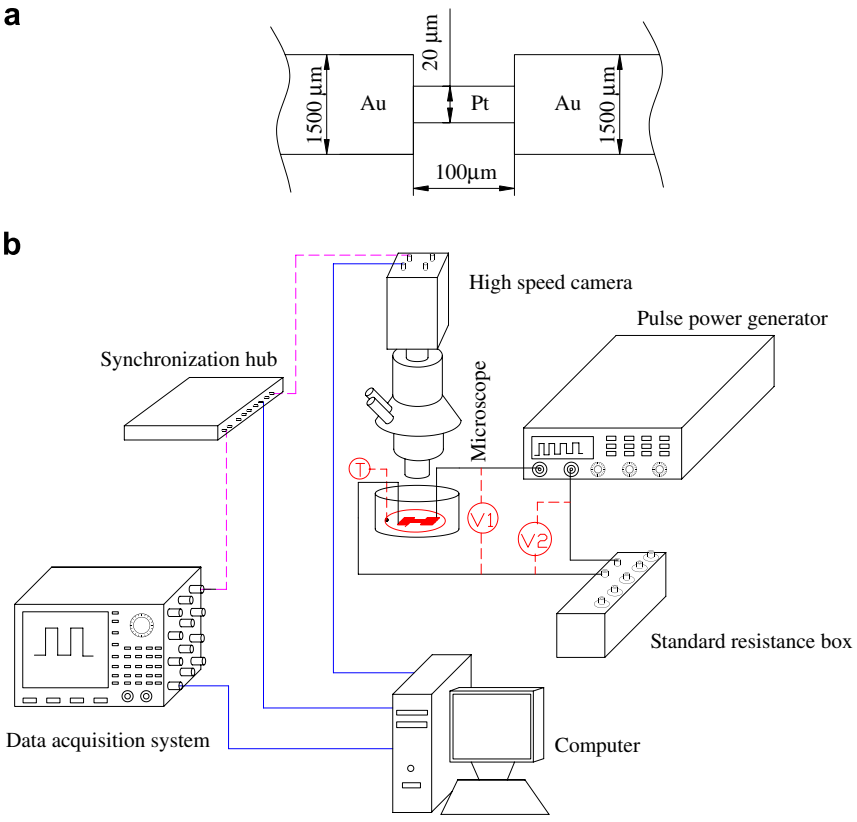

Fig. 1. The microheater and experimental setup.

the high speed data acquisition system to record the data, and the high speed camera to record the image files, simultaneously. The maximum time difference of the initial function of the two systems after they receive the trigger signal from the synchronization hub is less than 20 ns.

3. The microheater temperature calibration and data reduction

The whole microheater consists of the platinum film resistance of R_{Pt} and the two gold pad resistances of R_{Au1} and R_{Au2} (see Fig. 1a). At the room temperature, $R_{Pt} = 7.881\ \Omega$ and $R_{Au1} = R_{Au2} = 0.878\ \Omega$. During the calibration, the glass wafer is immersed in an oil beaker with the well controlled temperature. The oil temperature is measured by a precision thermocouple with the uncertainty of 0.2 °C and increased by 5 °C for each step. A low dc voltage is applied to the microheater and its connected resistance, maximally lowering the temperature increase of the microheater due to the Joule heating. V_1 and V_2 are measured by the data acquisition system instantaneously. Under the known resistances of R_{Au1}, R_{Au2} and R_s, the platinum film resistance can be computed as $R_{Pt} = V_1 R_s / V_2 - R_{Au1} - R_{Au2}$, corresponding to T_{Pt}. The repeated process yields a linear correlation of $T_{Pt} = 56.728 R_{Pt} - 314.8$. The calibrated temperature has the range from room temperature to 150 °C. Extension of the correlation to higher temperatures leads to acceptable accuracy due to its good linear behavior.

During the boiling experiment, the instantaneous measurements of V_1 and V_2 at any time step yields $R_{Pt}(t) = V_1(t) R_s / V_2(t) - R_{Au1} - R_{Au2}$, resulting in the computed microheater temperature according to the developed linear correlation in the calibration process. The electric circuit computation obtains the Joule heating power at the platinum surface as

$$Q(t) = \left(\frac{V_2(t)}{R_s}\right)^2 \left(\frac{V_1(t)}{V_2(t)} R_s - R_{Au1} - R_{Au2}\right) \quad (1)$$

The heat flux on the microheater is computed as $q(t) = Q(t)/(LW)$.

4. Uncertainty analysis

The three-dimensional simulations of platinum film and two gold pads were performed using FLUENT 6.0. The bottom surfaces of the metal films that are deposited on the glass substrate are adiabatic, while the surface that is exposed in the liquid has the convective boundary condition. The convective heat transfer coefficient between the exposed surface and the surrounding liquid is cited from Deng et al. [10]. The internal heat source is determined by the total voltage applied to the gold pads and the platinum film. It is shown that the temperature is uniform over the surface area larger than 80% of the whole platinum film heater. But the platinum film temperatures have a sharp drop at the junction interface of the platinum film and

the gold pads. At the given voltage of 20 mV applied to the whole microheater, the temperature rise of the platinum film beyond the liquid pool is computed to be 3 °C, due to the Joule heating effect. This is the maximum error that is encountered during the calibration process.

Now we estimate the uncertainties during the boiling experiment. According to Holman [11], if R is a given function of the independent variables of $x_1, x_2, x_3, \ldots, x_n$, $R = R(x_1, x_2, \ldots, x_n)$, and $\Delta x_1, \Delta x_2, \Delta x_3, \ldots, \Delta x_n$ are the uncertainties in these independent variables, the uncertainty of R can be evaluated by

$$\Delta R = \sqrt{\left(\frac{\partial R}{\partial x_1}\Delta x_1\right)^2 + \left(\frac{\partial R}{\partial x_2}\Delta x_2\right)^2 + \cdots\cdots + \left(\frac{\partial R}{\partial x_n}\Delta x_n\right)^2} \tag{2}$$

Giving the uncertainties of $\Delta V_1 = 1$ mV, $\Delta V_2 = 1$ mV, $\Delta R_s = 0.01\ \Omega$, $\Delta R_{Au1} = 0.1\ \Omega$, $\Delta R_{Au2} = 0.1\ \Omega$, and substituting Eq. (2) by $T_{Pt} = 56.728(V_1 R_s/V_2 - R_{Au1} - R_{Au2}) - 314.8$, the maximum uncertainty of the platinum film temperature is 8.08 °C. Similarly, the heat flux at the platinum film heater surface has the uncertainty of 6.0%.

5. Results and discussion

Three pulse heating parameters govern the bubble behaviors: the pulse frequency of f, the pulse heating duration time of τ_1, the pulse voltage amplitude of $V_1 + V_2$ during the period of τ_1. The cycle period is $T_{cycle} = 1/f = \tau_1 + \tau_2$. In the present study, τ_1/T_{cycle} is about 11% for all the runs.

We fix the pulse frequency, gradually increase $V_1 + V_2$, until bubbles can be observed by the optical system. Bubble behavior is observed to be dependent on f and $V_1 + V_2$. Here we present three typical runs representative of three types of bubble patterns.

5.1. Bubble explosion and regrowth pattern

The first type of bubble pattern, named as the bubble explosion and regrowth, occurs at lower heat flux that just triggers the boiling incipience of the microheater. Fig. 2a shows the temperature response of the platinum film heater versus time, corresponding to the heat flux of 16–18 MW/m^2. A "V" shape curve is observed close to the end of the duration time of τ_1, corresponding to the boiling incipience. The inflection point of the "V" shape curve is 187 °C (460 K), which is identified as the boiling incipience by the video image and agrees with the superheat limit of $0.9T_c = 461.3$ K, strongly indicating the homogeneous nucleation. The temperature of the platinum film is sharply decreased by around 20 °C after the boiling incipience is triggered.

The first image of Fig. 3a shows a bubble, which is not completely condensed from the previous pulse cycle and stayed on the microheater center until the "V" shape temperature curve appears for the current cycle. The liquid

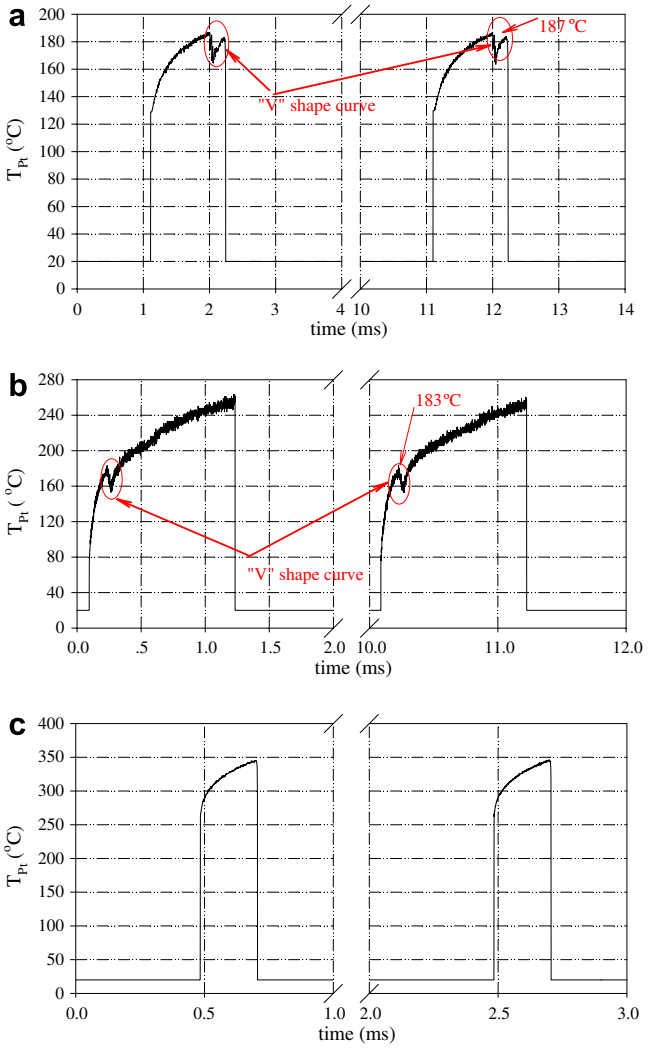

Fig. 2. Micro heater temperature response for three types of bubble phenomena. (a) $f = 100$ Hz, $\tau_1 = 1.130$ ms, $\tau_2 = 8.860$ ms, $\tau_1/T_{cycle} = 11.3\%$; (b) $f = 100$ Hz, $\tau_1 = 1.139$ ms, $\tau_2 = 8.853$ ms, $\tau_1/T_{cycle} = 11.4\%$; (c) $f = 500$ Hz, $\tau_1 = 0.22$ ms, $\tau_2 = 1.78$ ms, $\tau_1/T_{cycle} = 11.0\%$).

thickness between such bubble and the microheater surface consists of a hotter layer that is heated by the microheater, and the other colder layer that is not affected by the pulse heating. Because the bubble is not directly contacted with the hot liquid sub-layer on the microheater, such bubble does not influence the nucleation temperature for the current pulse cycle. The second image of Fig. 3a at $t = 12.05$ ms shows a large vapor cloud with the diameter of two times of the microheater length induced by the violent explosive boiling. Considering the half sphere of the vapor cloud with its diameter of two times of the microheater length, the surface area of the vapor cloud that is exposed in the subcooled liquid is thirty times of the microheater surface, thus the vapor cloud is instantaneously condensed and contracted to a smaller bubble at $t = 12.10$ ms in Fig. 3a, even though the microheater is still turned on. It is noted that only one image shows the explosive boiling due to the limited recording rate of our optical system.

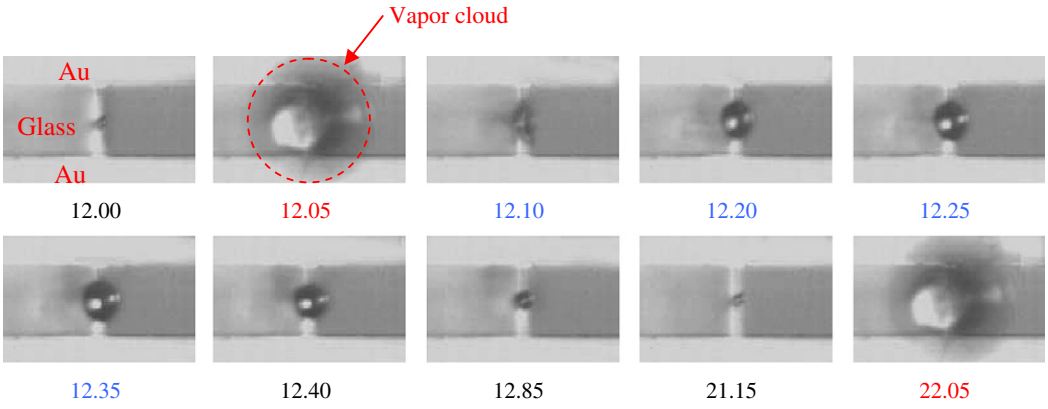

(a) the first type of bubble pattern

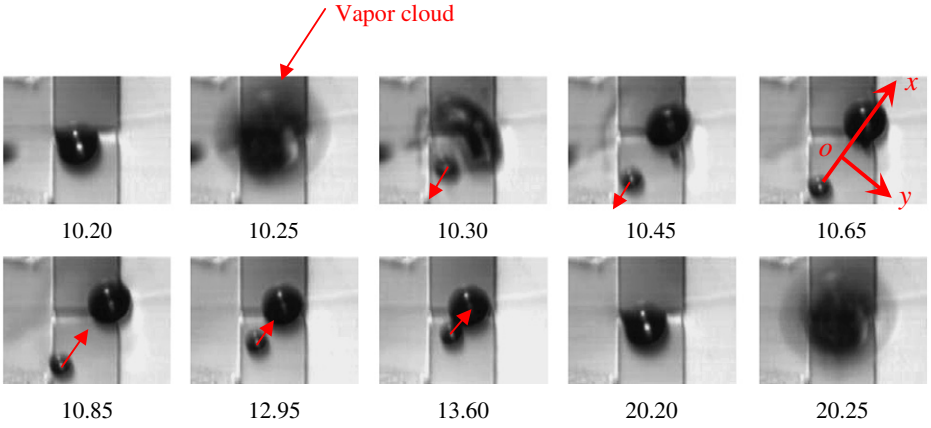

(b) the second type of bubble pattern

Fig. 3. The first and second types of bubble patterns (the unit is ms).

The continuous heating at the duration period of the pulse cycle ensures the bubble regrowth from the contracted bubble (see the images for 12.10 ms $< t <$ 12.35 ms in Fig. 3a). Note that the microheater is turned off at $t = 12.23$ ms but the bubble regrowth continues until at $t = 12.35$ ms. The heat stored in the solid substrate and the liquid sub-layer play an important role in the secondary bubble growth after the microheater was turned off. The subsequent bubble shrinking is observed for 12.40 ms $<$ $t <$ 22.00 ms in Fig. 3a after the microheater is off. The bubble regrowth phenomenon was also reported by Glod et al. [7] and Yin et al. [12].

5.2. Bubble breakup and attraction pattern

Increasing the voltage applied to the microheater yields the second type of bubble pattern: bubble breakup and attraction (see the images in Fig. 3b corresponding to the second heating pulse of Fig. 2b). The heat flux is 30–36 MW/m^2 at the duration time of τ_1 for such run case. The explosive boiling phenomenon is observed, which is similar to the first type of bubble pattern. However, due to much higher heat flux on the microheater, the violent explosive boiling breaks up the vapor cloud into two pieces (see the image at $t = 10.30$ ms in Fig. 3b). The broken pieces of the bubbles are moving away from the microheater due to the initial momentum caused by the explosive boiling.

The separated bubbles are observed to be attracted with each other. This can be seen in the images for 10.65 ms $< t <$ 20.20 ms in Fig. 3b. In order to explain the bubble attraction phenomenon, an attached coordinate was established. The x-coordinate is the connection line between the two bubbles. The y-coordinate is perpendicular to the center of the line of the two bubbles (see Fig. 3b). Because the separated bubbles are in the subcooled liquid, heat released by the condensed bubbles results in higher liquid temperature in the center region of the two bubbles, but it is decreased along the y-coordinate. The Marangoni effect causes liquid moving along the y-coordinate, leaving space to be occupied by the two bubbles. Thus, the two bubbles are moving toward each other. The bubble attraction process finally leads to the coalescence of the two bubbles at $t = 20.20$ ms in Fig. 3b.

5.3. Bubble size oscillation and large bubble formation pattern

The third type of bubble pattern is named as the bubble size oscillation and large bubble formation, occurring at

higher heat fluxes than those of the first and second types, or at higher pulse heating frequencies such as $f = 500$ Hz. When such pulse signal is applied to the microheater, the bubble dynamics is similar to that of the continuous heating. The heat flux is in the range of 20–22 MW/m^2 for the third type of bubble pattern (see Fig. 2c for the temperature response and Fig. 4 for the bubble behavior). The bubble nucleation only takes place for the first pulse signal. Because the whole process needs longer time in the order of 1 s, the sampling rate of the data acquisition system is lower than those for the first and second type of bubble patterns, limited by the internal memory of the data acquisition system. Thus the "V" shape curve of the ultra-fast temperature response for the first heating pulse is not captured by the data acquisition system (see Fig. 2c).

The process can be divided into three sub-stages. The video images for 44 ms $< t <$ 57 ms in Fig. 4a show a small and a large bubble occurring alternatively for a set of pulses (first stage). The general trend is the increased bubble size versus time, but it is still controlled by the pulse heating.

There is a critical bubble size above which the bubble continues to grow for $t >$ 57 ms in Fig. 4a (second stage).

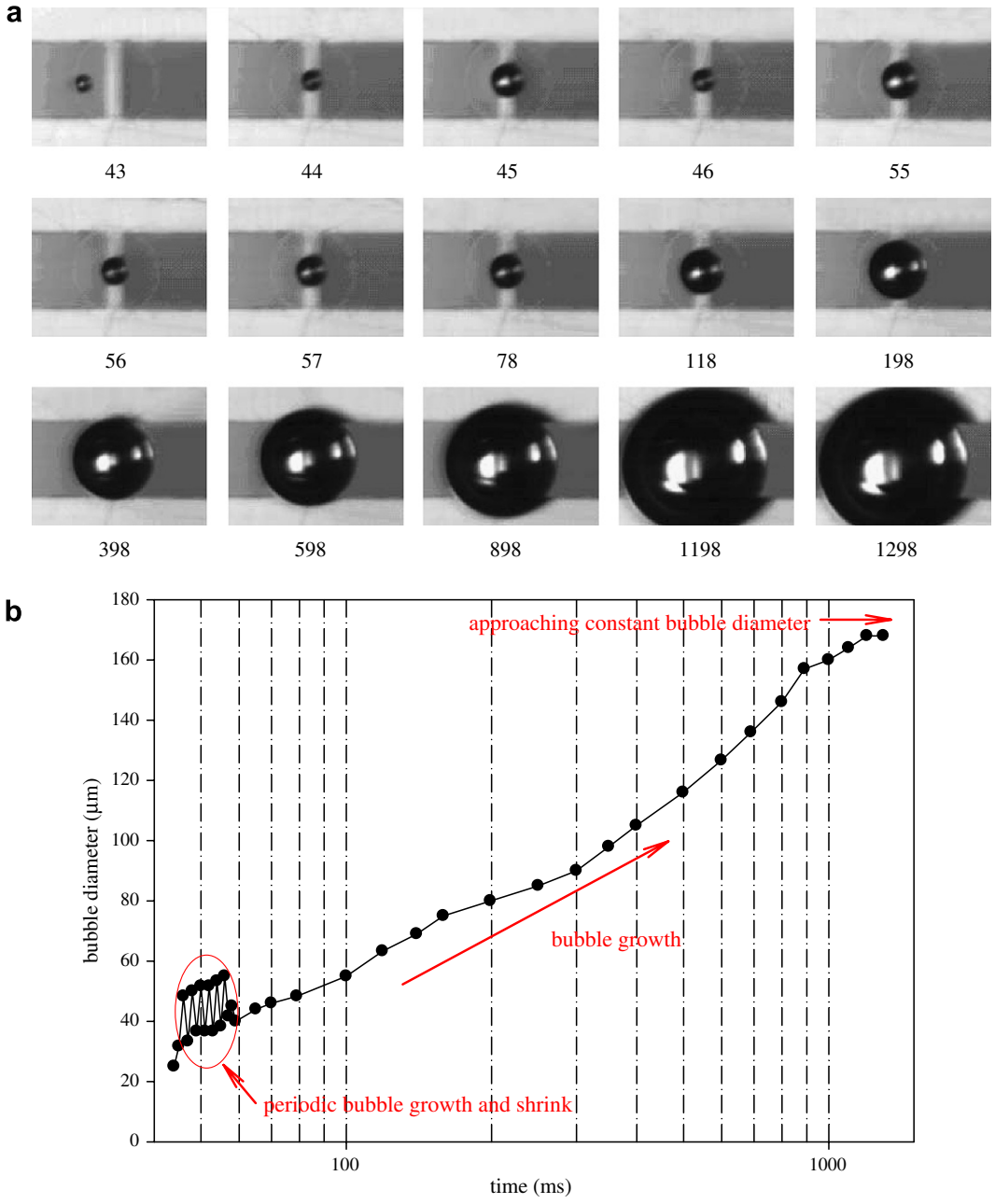

Fig. 4. The third type of bubble pattern and the bubble size versus time (the unit is ms).

The process is similar to that under the continuous heating condition with the equivalent heat flux of $\int_0^{\tau_1} q\mathrm{d}t/(\tau_1+\tau_2)$. The continuous bubble growth is due to the exceeded vapor mass provided by the microheater over the condensed vapor mass on the vapor–liquid interface. When the bubble size is increased to a value at which the condensed vapor is balanced by that produced by the microheater, the bubble attains its maximum size which is not changed versus time. This is the third sub-stage of the process.

The third type of bubble pattern is a dangerous one because the microheater temperature will be sharply increased if the balance between the produced and condensed vapor is broken. Under such circumstance, the critical heat flux condition is reached for the microheater. Fig. 4b shows the bubble size versus time during the whole process.

6. Comparison with other studies

We study effects of pulse heating parameters on the micro bubble behavior at a microheater surface. Three types of bubble patterns are observed, depending on the pulse heating parameters. Some of the experimental findings are consistent with those reported previously, but some of them are not reported in the literatures, to the authors' knowledge. These are described as follows.

One important issue is the boiling incipience temperature, depending on the surface roughness, non-condensable gas, and heating rates. We identified the boiling incipience occurring at the superheat limit of liquid, which is consistent with that reported by Asai [6] and Avedisian [13]. The bubble nucleation temperature was found to be higher than the superheat limit of liquid for the 3 μm width heater, and less than the superheat limit for the 5 μm width heater, reported by Lee et al. [14]. The temperature drop is identified to be about 20 °C covering the present data range, while the temperature was decreased by 8 °C, identified by Tsai and Lin [15].

Due to the high bubble nucleation temperature, the violent explosive boiling is observed in the present experiment. The explosive boiling and subsequent shrinking were also reported by Glod et al. [7] and Li et al. [8].

With increasing the heat fluxes on the microheater surface, the strong explosive boiling causes the breakup of the vapor cloud instantaneously after the vapor cloud is formed. The separated pieces of the vapor cloud move away from the microheater initially due to their initial momentum. But these pieces are attracted with each other due to the Marangoni effect induced by the temperature gradient which is perpendicular to the connection line between the two bubbles. This phenomenon was not reported before. Besides, the third type of bubble pattern (the periodic bubble size oscillation and large bubble formation), was the new experimental finding, taking place at sufficient high heat fluxes or pulse heating frequencies.

7. Conclusions

An experiment was conducted using a platinum microheater by the size of 100 μm in length and 20 μm in width. Methanol is used as the working fluid. The present experiment covers a wide range of pulse heating parameters. It is found that the micro bubble behavior can be characterized into three types, depending on the pulse heating parameters. The first type, named as the bubble explosion and regrowth, consists of a violent explosive boiling and shrinking, followed by a bubble regrowth and contraction process, occurring at lower heat flux that is just initiating the boiling incipience. The second type of bubble pattern, named as the bubble breakup and attraction, occurs at higher heat fluxes than those of the first type. The more violent explosive boiling causes the bubble breakup and emitted from the microheater due to their initial momentum. The Marangoni effect induces the liquid between the two bubbles moving away from the center of the line between the two bubbles, leaving the space for the two bubbles to be occupied. Thus the separated bubbles are moving toward each other. The bubble attraction process is over until the two bubbles are fully merged.

Much higher heat fluxes or pulse heating frequencies lead to the third type of bubble pattern: the bubble size oscillation and large bubble formation. The process involves a periodic bubble size oscillation, followed by a continuous increase of the bubble size, equivalent to the continuous heating mode, until a constant maximum bubble size is reached.

Acknowledgements

The work is supported by the National Natural Science Foundation of China (50476088), and the Natural Science Foundation of Guangdong Province (5000729).

References

[1] L.W. Lin, Thermal challenges in MEMS applications: phase change phenomena and thermal bonding processes, Microelectron. J. 34 (2003) 179–185.
[2] H. Tsai Jr., L. Lin, A thermal bubble actuated micro nozzle-diffuser pump, J. Microelectromech. Syst. 11 (2002) 665–671.
[3] H. Tsai Jr., L. Lin, Active microfluidic mixer and gas bubble filter driven by thermal bubble micropump, Sens. Actuators, A 97–98 (2002) 665–671.
[4] P.G. Deng, Y.K. Lee, P. Cheng, The growth and collapse of a microbubble under pulse heating, Int. J. Heat Mass Transfer 46 (2003) 4041–4050.
[5] J.M. Delhaye, J.B. Mclaughlin, Appendix 4: report of study group on microphysics, Int. J. Multiphase Flow 29 (2003) 1101–1116.
[6] A. Asai, Bubble dynamics in boiling under high heat flux pulse heating, ASME J. Heat Transfer 113 (1991) 973–979.
[7] S. Glod, D. Poulikakos, Z. Zhao, G. Yadigaroglu, An investigation of microscale explosive vaporization of water on an ultrathin Pt wire, Int. J. Heat Mass Transfer 45 (2002) 367–379.
[8] J. Li, G.P. Peterson, Microscale heterogeneous boiling on smooth surfaces – from bubble nucleation to bubble dynamics, Int. J. Heat Mass Transfer 48 (2005) 4316–4332.

[9] T.L. Chen, J.F. Klausner, S.V. Garimella, J.N. Chung, Subcooled boiling incipience on a highly smooth microheater, Int. J. Heat Mass Transfer 49 (2006) 4399–4406.
[10] P.G. Deng, Y.K. Lee, P. Cheng, An experimental study of heater size effect on micro bubble generation, Int. J. Heat Mass Transfer 49 (2006) 2535–2544.
[11] J.P. Holman, Experimental Methods for Engineers, fourth ed., McGraw-Hill, NY, 1984.
[12] Z. Yin, A. Prosperretti, J. Kim, Bubble growth on an impulsively powered microheater, Int. J. Heat Mass Transfer 47 (2004) 1053–1067.
[13] C.T. Avedisian, W.S. Osborne, F.D. Mcleod, C.M. Curley, Measurement bubble nucleation temperature on the surface of a rapidly heated thermal ink-jet heater immersed in a pool of water, Proc. R. Soc. London, Ser. A 455 (1999) 3875–3899.
[14] J.Y. Lee, H.C. Park, J.Y. Jung, H.Y. Kawk, Bubble nucleation on micro line heaters, J. Heat Transfer Trans. ASME 125 (2003) 687–692.
[15] J.H. Tsai, L.W. Lin, Transient thermal bubble formation on polysilicon micro-resisters, J. Heat Transfer Trans. ASME 124 (2002) 375.